scientific reports

Check for updates

OPEN

AAV.PHP.eB-based strategies for precise modulation of α7 nicotinic acetylcholine receptor in neurons and astrocytes in the adult mouse brain

Giulia Puliatti[1], Pietro Renna[1], Martina Battistoni[1,2], Roberto Piacentini[1,2], Cristian Ripoli[1,2,3]✉ & Claudio Grassi[1,2,3]

Precise control of the α7 nicotinic acetylcholine receptor (α7-nAChR) in specific brain cell types is crucial for understanding its role in neural circuit function and disease. Here, we introduce a set of AAV.PHP.eB-based gene delivery vectors optimized for cell-type-specific downregulation or overexpression of α7-nAChR in the adult mouse brain. Using promoters for neuronal or astrocytic targeting, we achieved efficient cell-type modulation of α7-nAChR after intra-hippocampal administration. These vectors provide a versatile platform for investigating α7-nAChR-dependent mechanisms in vivo and advancing the preclinical development of targeted interventions for neurological disorders characterized by receptor dysregulation.

Keywords α7-nAChR, shRNA, Gene delivery, Cell-type-specific

The α7 nicotinic acetylcholine receptor (α7-nAChR) is a ligand-gated ion channel abundantly expressed in the central nervous system, where it plays critical roles in neuronal signaling[1], synaptic plasticity[2], neuroinflammation[3] and cognitive processes[4]. Functionally, α7-nAChRs are characterized by Ca^{2+} permeability contributing to the modulation of neurotransmitter release, intracellular signaling cascades, and long-term synaptic potentiation[5]. Interestingly, α7-nAChR has been demonstrated to be expressed not only in neurons but also in astrocytes[6]. Altered α7-nAChR expression or function has been implicated in a range of neuropsychiatric and neurodegenerative disorders, including schizophrenia, Alzheimer's disease, and post-stroke inflammation, making it a promising therapeutic target for modulating both neurocognitive and neuroimmune degenerative pathways[7–9]. Despite growing interest in α7-nAChRs as therapeutic targets, selectively manipulating these receptors in specific cell types and brain regions remains technically challenging. These limitations have hindered mechanistic studies of α7-nAChRs in vivo and restricted the development of targeted interventions. Here, we developed a suite of AAV.PHP.eB-based vectors enabling cell-type-specific overexpression or knockdown of α7-nAChR in the mouse brain. Using the human synapsin (hSyn) promoter for neuronal targeting and glial fibrillary acidic protein (GFAP) promoter for astrocytic targeting, we achieved robust and selective α7-nAChR modulation following intracerebral delivery in adult C57BL/6 mice of 3 months of age. Validation by immunofluorescence co-labeling confirmed precise cell-type specificity while western blot (WB) analyses demonstrated significant modulation of endogenous α7-nAChR expression levels in vivo. We recently apply these vectors to investigate the synaptic consequences of α7-nAChR modulation[10]. However, the engineering strategy underlying shRNA design and screening, promoter-specific construct architecture, cross-system validation, and safety profiling was not described. The present study provides a systematic methodological framework detailing the rational development, optimization, and validation of AAV-PHP.eB-based tools for cell-type-specific modulation of CHRNA7. By establishing reproducible design principles and benchmarking across heterologous cells, primary cultures, organotypic slices, and adult brain, we extend beyond proof-of-concept application and define a standardized viral platform for future mechanistic and translational studies.The resulting tools enable efficient and flexible manipulation of α7-nAChR signaling in defined central nervous system (CNS) cell populations

[1]Department of Neuroscience , Università Cattolica del Sacro Cuore , 00168 Rome, Italy. [2]Fondazione Policlinico Universitario A. Gemelli IRCCS, 00168 Rome, Italy. [3]These authors contributed equally: Cristian Ripoli and Claudio Grassi. ✉email: cristian.ripoli@unicatt.it

facilitating preclinical evaluation of α7-nAChR-targeted therapeutic strategies in experimental models of brain disorders.

Materials and methods

Plasmid design and viral vector assembly for CHRNA7 overexpression or silencing

To generate plasmids capable of overexpressing CHRNA7 selectively in neurons and astrocytes, the CHRNA7 coding sequence from plasmid Addgene #62276 was amplified by PCR and inserted into two in-house pAAV2 viral backbones, containing the hSyn or GFAP promoters as well as mRuby2 gene reporter, using Gibson Assembly (Gibson Assembly Master Mix, New England Biolabs, Ipswich, MA, USA). pcDNA3.1-CMV-CHRNA7 was a gift from Sherry Leonard & Henry Lester (Addgene plasmid #62276[11]). All restriction enzymes were purchased from New England Biolabs.

In this way, we generated pAAV-hSyn-CHRNA7-mRuby2 and pAAV-GFAP-CHRNA7-mRuby2. Sequence verification was performed by Sanger sequencing. Data were analyzed using SeqScape Software (Version 2.7, Applied Biosystems, Thermo Fisher Scientific Inc., Waltham, MA, USA; available at: https://www.thermofisher.com/), supported by SnapGene (Version 6.2.2, GSL Biotech LLC, Chicago, IL, USA; available at: https://www.snapgene.com/).

For the silencing of endogenous CHRNA7, three different short hairpin RNAs (shRNA)-expressing plasmids were tested. Two constructs were purchased from VectorBuilder Inc. (Chicago, IL, USA):

1. pscAAV[shRNA]-mCherry-U6-mChrna7[shRNA#1];

   (shRNA sequence: GCAGTGGAACATGTCTGAGTA)

2. pscAAV[shRNA]-mCherry-U6-mChrna7[shRNA#2].

   (shRNA sequence: CAGATTTGGAAACCAGACATT)

These sequences were designed using proprietary software and expressed under the U6 promoter.

The third construct, pscAAV[shRNA]-EGFP-U6-{shRNA_CHRNA7#3}, contained a manually designed shRNA targeting sequence (TCTACTATGGCCTCAACCTGC).

After a functional validation, the latter home-made construct was chosen for further experimentation. To restrict silencing to neurons or astrocytes, the hSyn and GFAP promoters were PCR-amplified from the overexpression plasmids and inserted into pAAV2 viral backbones using Gibson Assembly. The final constructs, carrying mRuby2 as a reporter, were named pscAAV[shRNA]-hSyn-{CHRNA7_shRNA}-hSyn-mRuby2 and pscAAV[shRNA]-GFAP-{CHRNA7_shRNA}-GFAP-mRuby2, respectively.

Finally, all the overexpression and silencing plasmids were turned into adeno-associated viral vectors by InnovaVector s.r.l (Pozzuoli, Italy), generating the following four constructs:

AAV-PHP.eB-GFAP-shRNA_CHRNA7-GFAP-mRuby2;
AAV-PHP.eB-hSyn-shRNA_CHRNA7-hSyn-mRuby2;
AAV-PHP.eB-GFAP-CHRNA7-mRuby2;
AAV-PHP.eB-hSyn-CHRNA7-mRuby2.

The full sequences of the constructs are provided in the Supplementary Materials.

Design of CHRNA7-targeting shRNA sequence

Recent evidence has demonstrated the feasibility of expressing shRNAs under cell-type-specific type II promoters for targeted gene silencing in vivo[12]. Based on this, we designed shRNAs targeting the murine *CHRNA7* gene for selective silencing in neurons and astrocytes, by placing the shRNA expression cassettes under the control of the hSyn and GFAP promoters, respectively.

The murine CHRNA7 mRNA sequence (RefSeq: NM_007390.3) was used as a template. shRNA sequences were designed following the methodological guidelines described in literature[13,14]. In particular, target regions were selected within 50–100 nucleotides downstream of the start codon in the open reading frame, with a total length of 20–30 base pairs. In addition to these primary constraints, secondary structural rules were applied to increase silencing efficiency. The following empirical criteria were considered:

Rule 1: A/U at position 19, GC at position 1, A/U at position 10, > 3 A/Us between positions 13–19.
Rule 2: A/U at position 19, GC at position 1, GC at position 10, > 3 A/Us between positions 13–19.
Rule 3: G/C at position 19, GC at position 1, GC at position 11, > 6 A/Us between positions 5–19.
Rule 4: A/U at position 19, A/U at position 1, −3 A/Us between positions 13–19.

The shRNA molecule was assembled following the canonical structure: [Promoter]–[4 bp spacer]–[Sense sequence]–[Loop (6 bp)]–[Antisense sequence]–[Pol III terminator (TTTTT)].

The final sequence of the custom-designed shRNA was:

5'-TCTACTATGGCCTCAACCTGCTCAAGAGGCAGGTTGAGGCCATAGTAGA-3'.

Within this sequence, (i) the sense strand corresponds to TCTACTATGGCCTCAACCTGC, (ii) the loop is TCAAGAG, and (iii) the antisense strand is GCAGGTTGAGGCCATAGTAGA.

Immortalized cell line cultures and DNA transfections

HEK293T cells were a kind gift from Dr. Antonella Farsetti[15]. Cells were cultured in high glucose Dulbecco's modified Eagle's medium (DMEM, Sigma-Aldrich, St. Louis, MO, USA) supplemented with 10% (v/v) fetal bovine serum (FBS, Sigma) and incubated at 37 °C temperature and 5% CO_2 conditions. SH-SY5Y cells were cultured in DMEM/F12 (Sigma-Aldrich) medium supplemented with 10% (v/v) FBS and incubated at 37 °C temperature and 5% CO_2 conditions.

CHRNA7 overexpression or silencing was obtained transfecting both cell lines at 60 to 90% cell confluency with (pH 7.3) polyethylenimine HCl max solution (1 mg/ml; PEI max, Polysciences, Warrington, PA, USA with DNA plasmid vectors. Each cell culture dish containing 1×10^6 cells received a DNA-PEI max mixture consisting of 2.5 µg of total DNA along with 5 µg of PEI max in Opti-MEM Reduced Serum Media (Thermo Fisher Scientific, Waltham, MA, USA).

Ca^{2+} imaging

To perform Ca^{2+} imaging, SH-SY5Y cells were transfected either with plasmid carrying the CHRNA7 transgene or the plasmid carrying the shRNA targeting CHRNA7, as described in the previous paragraph. After 24 h from the transfection, transfected and control non-transfected SH-SH5Y cells were incubated for 30 min at 37 ◦C with 2.5 µM Fluo-4-AM (Thermo), a Ca^{2+} sensitive fluorescent dye, in Tyrode's solution. This solution consisted of NaCl (150 mM), glucose (10 mM), HEPES (10 mM), KCl (4 mM), $CaCl_2$ (4 mM) and $MgCl_2$ (1 mM) and its pH was adjusted to 7.4 with NaOH. Cells were then maintained in fresh Tyrode's solution at RT for 20 min to allow dye de- esterification. Intracellular Ca^{2+} transients were recorded for 5 consecutive minutes and were elicited by exposing Fluo-4-AM-loaded cells to 50 µM PNU-282,987 (Sigma) after 1 min from the start of the acquisition. Fluo-4-AM was excited at 470 nm and its emission signal was collected between 500 and 550 nm with a CARV II spinning-disk microscope (Crisel Instruments, Rome, Italy).

The amplitude of each Ca^{2+} signal was estimated in a semi- quantitative way by the following formula: $\Delta F/F = (F_t - F_{pre})/(F_{pre} - F_{bgnd})$, where F_t is the mean of fluorescence intensities measured in a region of interest (ROI) drawn around each cell body at a given time (t); F_{pre} is the basal fluorescence intensity in this ROI estimated as mean value of fluorescence during 1 min prior PNU exposure; F_{bgnd} is back ground fluorescence intensity measured in an area lacking dye-filled cells.

Animals

Wild-type (WT, C57BL/6J; RRID: IMSR_JAX:000664) mice were purchased from The Jackson Laboratory. Mice were located in the animal facility at Università Cattolica del Sacro Cuore. Hygrometric and thermic conditions were kept stable (50%; 21 ± 1 °C) on 12 h light/dark cycle, and animals had ad libitum access to food and water. To test the efficacy of the four different viral vectors, we used three mice per experimental group.

Ethics

All the experiments were performed following institutional animal welfare guidelines and legislation, approved by the local Institutional Animal care and Use Committee and the European Communities Council Directives (2010/63/EU) and the Italian Ministry of Health (authorization n° 944/2021-PR). All methods were performed in accordance with the relevant guidelines and regulations, and are reported in compliance with the ARRIVE guidelines.

Primary cultures of hippocampal and cortical neurons and astrocytes and viral infections

Primary co-cultures of hippocampal and cortical neurons and astrocytes were prepared from WT E18 C57BL/6 mice. In brief, after brain removal, cortices and hippocampi were placed in Phosphate Buffered Saline (PBS) at 4 °C and then incubated for 10 min at 37 °C in PBS containing trypsin–ethylenediaminetetraacetic acid 0.025%/0.01% (w/v, Trypsin-EDTA, Biochrom AG, Berlin, Germany). 1% FBS was used to inactivate trypsin, and the tissues were centrifugated and suspended in a dissociation medium consisting of 97.8% minimum essential medium (MEM, Biochrom), 1% FBS, 2 mM glutamine, 25 mM glucose and 1% penicillin–streptomycin-neomycin antibiotic mixture (PSN, Thermo). Tissues were then mechanically dissociated with a fire-polished Pasteur pipette at room temperature (RT) and then centrifuged at 800 × g for 10 min at RT. Cells were resuspended in the previously described medium added with 5% horse serum and 5% FBS and plated on poly-L-lysine (0.1 mg/mL, Sigma)-pre-coated 35-mm six-well plates (10^5 cells/well) for RNA or protein isolation.

After 24 h from seeding (1 day in vitro, DIV), the culture medium was replaced with a fresh medium consisting of 96.5% Neurobasal medium (Thermo), 2% B-27 (Thermo), 2 mM glutamine and 1% PSN. After 72 h (4 DIV), this medium was replaced with a glutamine-free version of the same medium, and the cells were grown for 10 more days before carrying-out experiments. Co-cultures were infected at 14 DIV with AAV-PHP.eB-GFAP-shRNA_CHRNA7-GFAP-mRuby2 or AAV-PHP.eB-hSyn-shRNA_CHRNA7-hSyn-mRuby2, at a concentration of 1 MOI (i.e., 1 genome copy/cell).

Organotypic hippocampal brain slices preparation, DNA transfection, and viral infections

Hippocampal organotypic slice cultures were prepared from WT P2-8 C57BL/6 mice using a McIllwain tissue chopper, using at least 4 mice for each preparation. Slices 300 µm thick were placed on semi-porous membranes (Merck Millipore, No. PCIMORG50, Burlington, MA, USA) and fed by tissue medium made of MEM (Thermo) supplemented with 30 mM HEPES, 26.6 mM D-glucose, 5.8 mM $NaHCO_3$, 2 mM $MgSO_4$, 1 mM $CaCl_2$, 0.5 mg/mL insulin, 2.5% ascorbic acid, 20% horse serum (Thermo). Slices were incubated at 36 °C in 5% CO2.

Hippocampal organotypic slices were either transfected by gene gun with DNA plasmid carrying the sequence of the shRNA targeting CHRNA7, or infected with viral constructs carrying the same sequences at a concentration of 3×10^9 gc.

RNA isolation and RT-qPCR

HEK293T and SH-SY5Y cultures were scraped and collected in Trizol reagent (Thermo) and total RNA was isolated according to the manufacturer's instructions. For each sample, 0.5 µg of RNA were retrotranscribed using the High-capacity cDNA reverse transcription kit (Applied Biosystems, Foster City, CA, USA). The

expression of the transcripts was evaluated by real time quantitative PCR, performed with Power SYBR™ Green PCR Master Mix (Applied Biosystems) on Applied Biosystems 7500 thermocycler using the following primers:

CHRNA7 Fw 5' – ACATGCGCTGCTCGCCGGGA – 3'

Rv 5' – GATTGTAGTTCTTGACCAGCT – 3'

GAPDH Fw 5' – CATGAGAAGTATGACAACAGCCT – 3'

Rv 5' – AGTCCTTCCACGATACCAAAGT – 3'

RT-scPCR

CHRNA7 mRNA expression in single neurons of hippocampal brain slices (transfected with plasmid carrying the shRNA targeting CHRNA7) was assessed by single cell quantitative PCR. Single cell contents from transfected (fluorescent) neurons were collected as previously described[16,17]. Briefly, presterilized glass electrodes were filled with Rnase-free intracellular solution containing 1 U/μL recombinant Rnase inhibitor (Ambion, Austin, TX, USA) and then used to obtain whole cell patches on neurons in hippocampal slices. The intracellular contents (~4–5 μL) were drawn into the tip of the patch pipette by applying negative pressure and were then transferred to RNase/DNase-free tubes. The volume in each tube was brought up to 10 μL by adding Single Cell DNase I/Single Cell Lysis solution of Single Cell-to-CT kit (Life Technologies, Grand Island, NY, USA), and then the contents were incubated at room temperature for 5 min. Following cDNA synthesis by performing reverse transcription in a thermal cycler (25 °C for 10 min, 42 °C for 60 min, and 85 °C for 5 min), CHRNA7 gene expression primers were added to preamplification reaction mix based on the instructions from the kit (95 °C for 10 min, 14 cycles of 95 °C for 15 s, 60 °C for 4 min, and 60 °C for 4 min). The products from the preamplification stage were used for the real time qPCR reaction (50 °C for 2 min, 95 °C 10 min, and 40 cycles of 95 °C for 5 s and 60 °C for 1 min) on Applied Biosystems 7500 thermocycler with validated probes designed to detect CHRNA7 (Mm01312230_m1 TaqMan probe). CHRNA7 mRNA levels were normalized to the housekeeping gene 18 S (Hs99999901_s1 TaqMan probe) and analyzed by using the $2-\Delta\Delta Ct$ method. Also, the transcript levels of CACNA1c gene (Mm00437917_m1 TaqMan probe) were assessed, and used as neuron-specific controls.

In vivo viral infections

Three-month old WT were anesthetized (80–100 mg/kg ketamine + 5–10 mg/mL xylazine) and placed in the stereotaxic frame. AAV-PHP.eB vectors were inoculated in the dorsal hippocampus at the following coordinates (2 μL/region, corresponding to 3×10^9 gc for each region): dorsal CA1–2.1 AP; ± 1.8 ML; −1.5 DV, dorsal CA2–2.1 AP; ± 2.2 ML; − 1.9 DV and dorsal CA3–2.1 AP; ± 2ML; − 2.1 DV as described elsewhere[10]. At the end of the procedure, the surgical wound was sutured, and the animals were administered with saline solution (≈ 200 μL/mouse) via intramuscular injection. In some mice, AAV-PHP.eB vectors were injected only in one hemisphere, in order to leave the contralateral as internal control (injected with saline only). Three weeks after the injection, some mice were sacrificed by intracardiac perfusion of PFA and their brain cut and analyzed through immunofluorescence analysis in order to verify the distribution of the injected virus, while some others were sacrificed by cervical dislocation and their brain collected for Western blot analysis. According to this in vivo infection protocol, the efficiency of viral infection was of~85%, that we assessed by immunohistochemistry counting double positive cells ($NeuN^+$/$mRuby2^+$ and $GFAP^+$/$mRuby2^+$).

Immunohistochemistry

Immunofluorescence analyses were performed on coronal sections (40 μm thick) of perfused brains as well as PFA-fixed hippocampal organotypic slices. The sections were incubated for 1 h at RT in a blocking solution consisting of 1% bovine serum albumin, 10% normal goat serum, and 0.5% Triton X-100. Immunohistochemistry was performed on free-floating sections by using overnight at 4 °C the following antibodies: mouse anti GFAP antibody (#3670, 1:300, Cell Signaling) and anti-mouse NeuN (MAB377, 1:300, Millipore). The fluorescent secondary antibody Alexa Fluor 488 donkey anti-mouse (A32723, Invitrogen; 1:500) was then used for 90 min at RT. Cell nuclei were counterstained with DAPI (0.5 μg/mL) and the sections were mounted on glass slides and coverslipped with ProLong Gold antifade reagent. Confocal stacks of images were acquired with a confocal laser scanning system Nikon A1MP.

Protein isolation and western blot

Cells cultures, hippocampal organotypic slices, and brain tissues (hippocampus, neocortex) infected with each tested viral vector were lysed in RIPA buffer, supplemented with 1 mM phenylmethylsulphonyl fluoride (PMSF), sodium fluoride (NaF), sodium orthovanadate (NaVO), and protease inhibitor (PI) mixture. Then, they were sonicated and centrifuged at 13,000 × g for 20 min at 4 °C. The BCA Assay Kit (Thermo) was used to quantify the protein concentration of the lysates. For each sample, an equivalent amount of protein (30 μg) was loaded onto 8–12% tris-glycine polyacrylamide gel for electrophoresis separation. Proteins were electroblotted onto nitrocellulose membranes and then blocked with 5% non-fat dry milk in tris-buffered saline containing 0.1% Tween-20 for 1 h at RT. Membranes were incubated with the following primary antibodies: anti-rabbit nicotinic acetylcholine receptor alpha 7 antibody (ab216485, Abcam) and anti-mouse GFAP (#3670, Cell Signalling), all used at dilution 1:1,000, overnight at 4 °C. Anti-mouse GAPDH (#ab8245, Abcam; 1:1,000) and Ponceau S Solution (Thermo) were used as housekeeping proteins. Membranes were then incubated with appropriate secondary horseradish peroxidase (HRP)-conjugated antibodies diluted at 1:5,000 (anti-rabbit #7074, anti-mouse #7076; Cell Signalling) for 1 h at RT. The signal detection was performed with WESTAR ECL ETA C ULTRA 2.0 (XLS075, Cyanagen, Bologna, Italy), using UVItec Cambridge Alliance. Molecular weights for immunoblot analysis were determined through Precision Plus Protein™ Standards (BioRad, Hercules, CA, USA).

The densitometric analysis was carried out with UVItec Alliance 1D software (Version 16.08a, UVITEC Ltd., Cambridge, UK; available at: https://www.uvitec.co.uk/).

Statistics

Statistical comparisons and analyses were carried out with SigmaPlot software (Version 14.0; Systat Software Inc., San Jose, CA, USA; available at: https://systatsoftware.com/products/sigmaplot/).

Data samples were expressed as mean ± standard error of the mean (SEM). Kruskal-Wallis non-parametric test was used to compare three or more experimental groups (< 10 observations/group). The level of significance (p) was set at 0.05.

Results

In vitro assessment of plasmids and viral vector assembly

To manipulate the expression of the α7-nAChR, we first tested plasmid constructs designed to induce either overexpression or downregulation of CHRNA7 in heterologous cells. The CHRNA7-expressing plasmid, under a CMV promoter, was co-transfected with DsRed2 to evaluate the efficacy of transfection. Downregulating CHRNA7-plasmids contained mCherry or EGFP as a tag to evaluate the transfection of target cells (Fig. 1a). Quantitative PCR analysis performed 24 h post-transfection confirmed a robust upregulation of CHRNA7 mRNA in both HEK293T and SH-SY5Y cells transfected with the CHRNA7 expression cassette, increasing greater than 10,000-fold compared to non-transfected controls (Fig. 1b). We next evaluated four shRNA constructs targeting CHRNA7, including two customized by VectorBuilder (shRNA_CHRNA7#1, shRNA_CHRNA7#2) and one

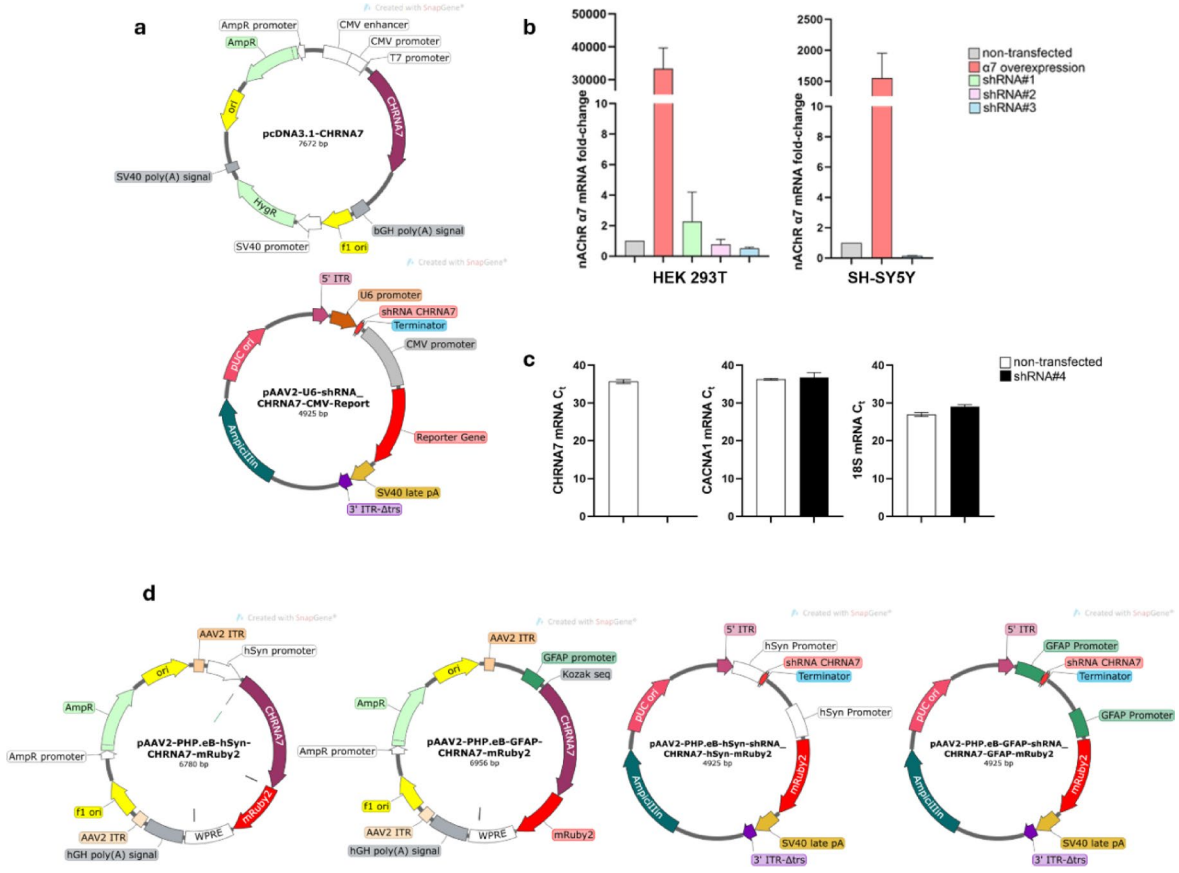

Fig. 1. Plasmids design and vector assembly. (**a**) Schematic representation of plasmids designed for overexpression (left) and downregulation (right) of CHRNA7 in HEK293T and SH-SY5Y cells. (**b**) Bar graphs representing the fold induction of CHRNA7 mRNA in HEK293T cells (treated as follow: non-transfected, transfected with overexpressing CHRNA7 plasmid, and transfected with each downregulating CHRNA7 plasmids) and in SH-SY5Y cells (treated as follow: non-transfected, transfected with overexpressing CHRNA7 plasmid, and transfected with the in-house downregulating CHRNA7 plasmid). Each graph shows the results obtained by three independent experiments. (**c**) Bar graph representing the CHRNA7 mRNA C_T in transfected and non-transfected CA1 pyramidal neurons from organotypic hippocampal slices transfected with pscAAV[shRNA]-EGFP-U6-{shRNA_CHRNA7#4}. CACNA1 and 18 S genes were used as specificity and loading controls. (**d**) Schematic representation of the final adeno-associated viral vectors, carrying the CHRNA7 gene or the shRNA_CHRNA7 sequences under the control of astrocyte-specific (GFAP) or neuron-specific (hSyn) promoters.

generated in-house (shRNA_CHRNA7#3). The first sequence, shRNA_CHRNA7#1, was designed to silence the murine isoform of the receptor and aligns suboptimally with human genomic DNA; however, based on the existing literature, partial mismatches can still support effective knockdown when thermodynamic and positional constraints are preserved[18,19]. The sequences of shRNA_CHRNA7#2 and shRNA_CHRNA7#3 completely targeted both the murine and the human isoforms of the receptor. We found that only shRNA_CHRNA7#2 and shRNA_CHRNA7#3 efficiently reduced CHRNA7 cDNA levels to 0.77 ± 0.47, and 0.52 ± 0.07, respectively, when normalized to 1.00 in non-transfected cells (Fig. 1b). On the contrary, the transfection with shRNA_CHRNA7#1 resulted in a slightly increased CHRNA7 transcript abundance (2.72 ± 2.27, Fig. 1b). To further validate the efficacy of the in-house shRNA construct (shRNA_CHRNA7#3) we repeated the experiments on SH-SY5Y cells. In this case, we also observed a significant reduction in CHRNA7 mRNA levels after transfection (0.15 ± 0.02, normalized to 1.00 in non-transfected cells; Fig. 1b). Based on the silencing efficiency, the in-house shRNA construct (shRNA_CHRNA7#3) was selected for subsequent experiments. To assess the silencing effect in a more physiologically relevant context, organotypic hippocampal slices derived from C57BL/6 mouse pups were transfected with the shRNA_CHRNA7#3 plasmid using a Gene Gun approach[20–22]. After 48 h, individual pyramidal neurons in the CA1 region were isolated under a fluorescence microscope, using EGFP expression to distinguish between transfected and non-transfected cells, which served as controls. Single-cell quantitative PCR analysis revealed that EGFP-positive neurons exhibited no detectable CHRNA7 mRNA. In contrast, expression of the housekeeping gene 18 S and the voltage-gated Ca^{2+} channel gene CACNA1c were preserved, confirming both the specificity and efficacy of the knockdown (Fig. 1c and Suppl. Fig. S1). Following identification of the optimal constructs for CHRNA7 modulation, the CHRNA7 coding sequence and shRNA_CHRNA7#3 cassette were cloned under the neuron-specific (hSyn) or astrocyte-specific (GFAP) promoters in plasmids containing the reporter gene mRuby2 (Fig. 1d). Plasmid assembly was performed using Gibson assembly, and the constructs were verified by Sanger sequencing. The resulting sequences were packaged into adeno-associated viral vectors (AAV-PHP.eB), generating the following AAVs: AAV-PHP.eB-GFAP-CHRNA7-mRuby2 and AAV-PHP.eB-hSyn-CHRNA7-mRuby2 for overexpression, and AAV-PHP.eB-GFAP-shRNA_CHRNA7-GFAP-mRuby2 and AAV-PHP.eB-hSyn-shRNA_CHRNA7-hSyn-mRuby2 for knockdown experiments (Fig. 1d).

As a functional correlate of the modulation of α7-nAChR across our designed constructs, we performed Ca^{2+} imaging on SH-SY5Y cells in which receptor expression was either upregulated or downregulated by transfection with the respective plasmids. SH-SY5Y cells transfected with the plasmid carrying the CHRNA7 transgene exhibited Ca^{2+} transients of greater amplitude upon stimulation with the receptor-selective agonist PNU-282987 compared to non-transfected cells. Conversely, the Ca^{2+} transients elicited in shRNA-transfected SH-SY5Y were lower compared to the control cells. In particular, in response to PNU stimulation, Ca^{2+}-dependent fluorescence increased by + 67.7 ± 7.4% in non-transfected cells, by + 107.0 ± 32.9% in CHRNA7-overexpressing cells, and by + 32.7 ± 12.0% in shRNA-transfected cells ($p = 0.0368$, assessed by Kruskal-Wallis test; Suppl. Fig S2).

In vivo CHRNA7 overexpression

To evaluate the cell-type-specific expression of CHRNA7 in vivo, 3-month-old C57BL/6 mice were intrahippocampally injected with either AAV-PHP.eB-GFAP-CHRNA7-mRuby2 or AAV-PHP.eB-hSyn-CHRNA7-mRuby2 targeting the dorsal CA1, CA2, and CA3 hippocampal regions (Suppl. Fig. S3a). Three weeks post-infection, immunofluorescence analyses were performed to verify transduction efficiency and specificity. Robust red fluorescence resulting from mRuby2 expression was detected throughout the hippocampi of all injected animals, indicating successful infection and transgene expression ($n = 3$ for AAV-PHP.eB-GFAP-CHRNA7-mRuby2; $n = 3$ for AAV-PHP.eB-hSyn-CHRNA7-mRuby2; mice weight ranged from 24.5 to 25.6 g and no significant changes were observed following infection). In sections from mice injected with AAV-PHP.eB-hSyn-CHRNA7-mRuby2, red fluorescence (mRuby2) was observed predominantly in cells with morphological features characteristic of neurons (Fig. 2a), that were indeed also stained by NeuN. Conversely, in animals receiving AAV-PHP.eB-GFAP-CHRNA7-mRuby2, red fluorescence (mRuby2) was mainly detected in GFAP-positive astrocytes (Fig. 2c).

Higher-magnification images confirmed the specificity of mRuby signal overlap with NeuN immunoreactivity in AAV-PHP.eB-hSyn-CHRNA7-mRuby2 infected mice and with GFAP in AAV-PHP.eB-GFAP-CHRNA7-mRuby2 infected mice, with negligible off-target expression detected outside the expected cell populations (Fig. 2b,d).

These results validate that both AAV constructs effectively transduced hippocampal cells with promoter-restricted expression patterns and establish a reliable system for cell-type-specific expression of CHRNA7.

In vitro CHRNA7 silencing

To investigate the efficacy of CHRNA7 knockdown in vitro, we used co-cultures of primary hippocampal neurons and astrocytes derived from C57BL/6 mouse embryos (E18). Cells were plated at a 1:1 neuron-to-astrocyte ratio and maintained for 14 days in vitro (DIV). Cultures were then infected with either AAV-PHP.eB-GFAP-shRNA_CHRNA7-GFAP-mRuby2 or AAV-PHP.eB-hSyn-shRNA_CHRNA7-hSyn-mRuby2 at a multiplicity of infection (MOI) of 1. One week later (DIV 21), cultures were processed for immunofluorescence and WB analyses to assess α7-nAChR subunit expression. Confocal imaging was used to detect red fluorescence in infected cells, confirming successful transduction by both vectors (Fig. 3a). To demonstrate cell-specific targeting, we infected organotypic hippocampal slices (then containing both neurons and astrocytes) with both AAVs (hSyn or GFAP) and labelled them for NeuN and GFAP, respectively (Suppl. Fig. S4). Quantification of protein levels revealed that infection with either the astrocyte-targeting or neuron-targeting shRNA vector significantly reduced the abundance of the α7-nAChR subunit compared to non-infected controls. Specifically, normalized protein expression decreased from 1.00 ± 0.17 in control cultures to 0.41 ± 0.04 in GFAP-shRNA-infected cultures and 0.45 ± 0.17 in hSyn-shRNA-infected cultures ($n = 5$ per condition; $p = 0.006$ and $p = 0.030$ vs. control, respectively,

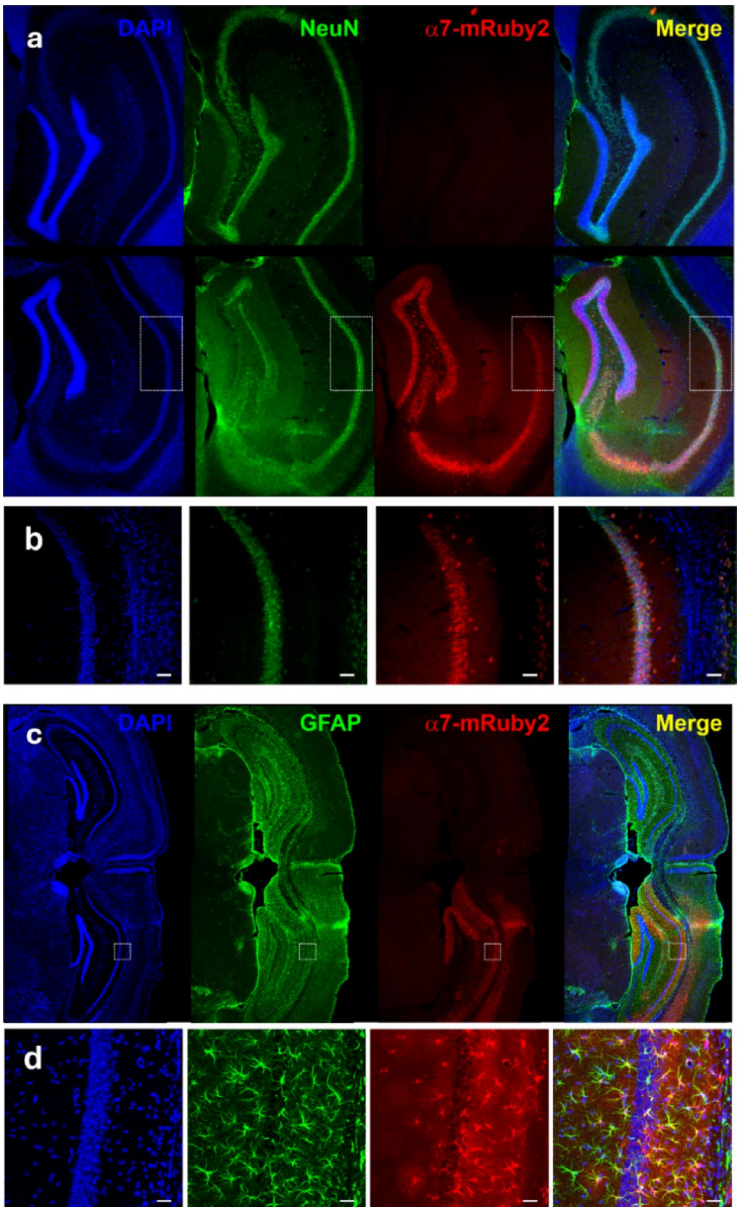

Fig. 2. CHRNA7 overexpressing AAVs selectively infect neurons and astrocytes in mice hippocampi. (**a**) Representative confocal image of the hippocampus of mice infected with AAV-PHP.eB-hSyn-CHRNA7-mRuby2. (**b**) Higher magnification of the white dotted box in the hippocampus showed in (**a**). (**c**) Representative confocal image of the hippocampus of mice infected with AAV-PHP.eB-GFAP-CHRNA7-mRuby2. (**d**) Higer magnification of the white dotted box in the hippocampus showed in (**c**).

assessed by Student's t test) (Fig. 3b). These findings demonstrate that both AAV constructs effectively mediate CHRNA7 knockdown in their respective target cell populations within mixed primary cultures.

In vivo CHRNA7 silencing

To assess the in vivo effectiveness and specificity of CHRNA7 knockdown, we performed stereotaxic intra-hippocampal injections in 3-month-old C57BL/6 mice using the same approach employed for the overexpression experiments. Animals received either AAV-PHP.eB-GFAP-shRNA_CHRNA7-GFAP-mRuby2 or AAV-PHP.eB-hSyn-shRNA_CHRNA7-hSyn-mRuby2 by intra-hippocampal injection in the dorsal CA1, CA2, and CA3 regions ($n = 3$/experimental group; mice weight ~25 g, Suppl. Fig. S3b)After three weeks, brains were collected and processed for immunofluorescence analysis to evaluate transduction efficiency and cell-type distribution of the transgene. The mRuby2 reporter fluorescence was consistently detected in the hippocampal regions of all injected animals, confirming successful delivery of the viral constructs. In the GFAP-shRNA group, mRuby2-positive cells had morphological features characteristic of astrocytes, demonstrating selective targeting of astrocytes (Fig. 4a,b). Conversely, in mice treated with the hSyn-shRNA vector, mRuby2 fluorescence was localized in cells resembling neurons in CA and DG regions, indicating neuron-restricted transduction (Fig. 4c,d). Minimal

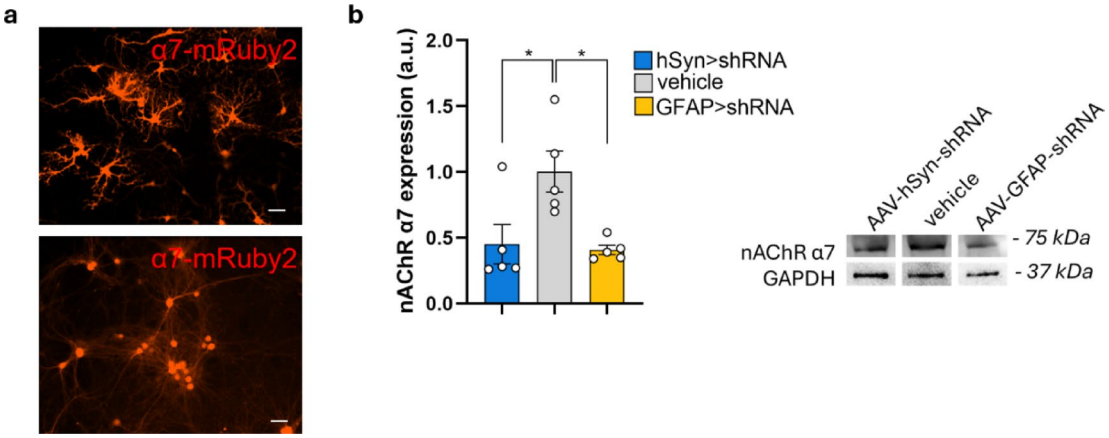

Fig. 3. CHRNA7 silencing AAVs efficiently reduce α7-nAChR protein levels in in vitro system. (**a**) Representative images of primary co-cultures of neurons and astrocytes infected either with AAV-PHP.eB-GFAP-shRNA_CHRNA7-GFAP-mRuby2 (up) or with AAV-PHP.eB-hSyn-shRNA_CHRNA7-hSyn-mRuby2 (bottom). Scale bar: 10 µm. (**b**) Representative WB analysis and relative bar graph showing the reduction of CHRNA7 in primary co-cultures treated as in (**a**) compared to the controls. GAPDH was used as loading control. The three different lanes derived from the same cropped blot (see Supplementary information - uncropped gels). The graph shows the results obtained by three independent experiments.

expression was observed outside the expected cell populations. Overall, these results establish that both AAV vectors mediated efficient, cell-type-specific expression of CHRNA7-targeting shRNA in vivo, providing a reliable strategy for selective gene silencing in the hippocampus.

Absence of gliosis after AAV-PHP.eB infection

Infection with AAV-PHP.eB may result in glial activation as a consequence of viral vector exposure and the associated innate immune response[23]. To evaluate whether our AAV-PHP.eB for CHRNA7 modulation were associated with gliosis in our in vitro and in vivo experimental models, we examined GFAP protein levels by WB analysis. Specifically, we assessed co-cultures of primary neurons and astrocytes infected with the shRNA-expressing vectors, as well as hippocampal and cortical tissue lysates collected from mice treated with each AAV construct. Quantitative analysis revealed no significant differences in GFAP expression between infected samples and their respective non-infected controls (Fig. 5). These findings indicate that under the conditions tested, AAV-PHP.eB-mediated CHRNA7 knockdown did not elicit detectable glial activation.

Discussion

The α7-nAChR is a homopentameric acetylcholine receptor[24] abundantly expressed in brain regions critical for memory and cognition, including the hippocampus and amygdala, where it is primarily localized on pyramidal neurons and astrocytes[4,25]. Understanding the function of α7-nAChR in both neurons and astrocytes is essential, as this receptor plays distinct and complementary roles in regulating neurotransmission, synaptic plasticity, and neuroimmune signaling across these cell types[26]. Elucidating how α7-nAChR contributes to neural circuit function and homeostasis across cellular contexts is crucial for understanding its role in cognitive processes and neuroinflammatory responses. Despite extensive research implicating α7-nAChR dysregulation in multiple brain disorders, there has been a need for strategies that enable precise, cell-type-specific manipulation of receptor expression in vivo. Such approaches are indispensable for disentangling the receptor's diverse functions and identifying therapeutic windows for intervention.

In this study, we developed and validated AAV.PHP.eB-based CHRNA7 gene delivery vectors enabling precise, cell-type-specific modulation of the α7-nAChR in neurons and astrocytes. Our results demonstrate the feasibility of achieving robust overexpression or knockdown of CHRNA7 in cultured cells (Fig. 3) and adult mouse brain (Figs. 2 and 4).

In vitro experiments confirmed that plasmids encoding the CHRNA7 expression cassette drove marked upregulation of receptor mRNA (10,000-fold increase), consistent with efficient transgene expression (Fig. 1). Among the shRNA constructs screened, we identified sequences that effectively reduced CHRNA7 mRNA levels showing consistent silencing efficiency across HEK293T and SH-SY5Y cells, primary co-cultures of neurons and astrocytes, and organotypic hippocampal slices (Figs. 1 and 3, and Suppl. Fig. 4). The rigorous validation pipeline adopted here strengthens the biological interpretation of our previous findings[10] and enhances the reliability of the generated vectors. While Cannata et al. focused on the physiological consequences of α7-nAChR deletion, the current study establishes the technical foundation of the viral system itself. Specifically, we describe the rationale for shRNA sequence selection, comparative screening across multiple candidate constructs, promoter-restricted architecture enabling neuron- or astrocyte-specific modulation, and validation across multiple experimental systems, including inflammatory safety assessment. These methodological aspects were not previously reported and are essential for reproducibility and broader application of the platform.

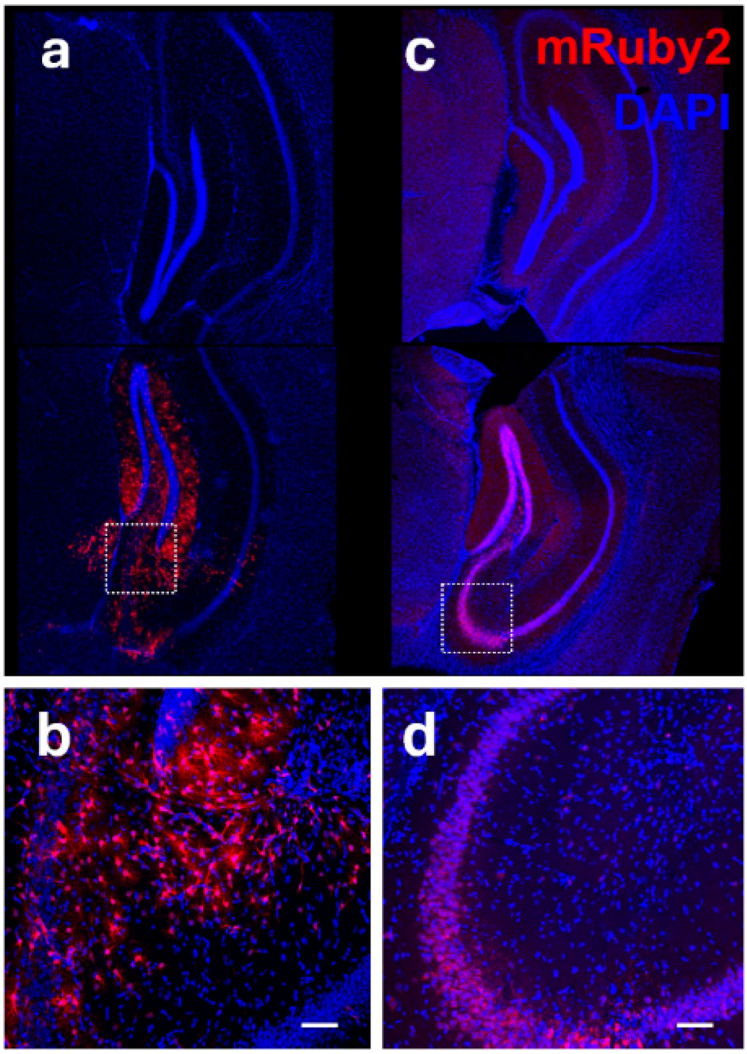

Fig. 4. CHRNA7 silencing AAVs selectively target neurons and astrocytes in mice hippocampi. (**a**) Representative confocal image of the hippocampus of mice infected with AAV-PHP.eB-GFAP-shRNA_CHRNA7-GFAP-mRuby2. (**b**) Higher magnification of the white dotted box in the hippocampus showed in (**a**). (**c**) Representative confocal image of the hippocampus of mice infected with AAV-PHP.eB-hSyn-shRNA_CHRNA7-hSyn-mRuby2. (**d**) Higher magnification of the white dotted box in the hippocampus is shown in (**c**). Scale bar: 50 μm.

Recent advances in AAV vector engineering have enabled systemic delivery approaches capable of crossing the blood-brain barrier and achieving widespread CNS transduction[27]. In particular, AAV.PHP.eB has emerged as a promising platform for gene therapies targeting the brain, offering high transduction efficiency with minimal invasiveness and the potential for broad distribution throughout neural tissue after intravenous administration[28].

The successful assembly of AAV.PHP.eB vectors incorporating either the neuronal (hSyn) or astrocytic (GFAP) promoters provided an efficient platform for targeting defined cell populations (Fig. 3). Following intrahippocampal delivery in vivo, immunofluorescence analyses demonstrated that the expression of mRuby2 reporter colocalized precisely with either NeuN or GFAP, confirming high specificity for neurons and astrocytes, respectively (Fig. 2). Importantly, our experiments did not detect evidence of gliosis induced by viral infection, as indicated by unchanged GFAP protein levels relative to controls (Fig. 5). This finding suggests that the AAV.PHP.eB-based vectors are well tolerated in vivo, supporting their suitability for long-term studies.

Collectively, these results establish that AAV.PHP.eB vectors can drive significant and selective modulation of α7-nAChR expression across multiple model systems. Such tools provide critical advantages over pharmacological approaches, including the ability to achieve long-lasting effects with cell-type specificity and minimal off-target impacts. In particular, the combination of the PHP.eB capsid's enhanced CNS tropism[28] and the use of cell-restricted promoters enables efficient transduction of broad brain regions while maintaining precise control over the targeted population.

The availability of these vectors has important implications for both basic and translational neuroscience research. In mechanistic studies, they can be applied to dissect the roles of α7-nAChR in synaptic plasticity, neuroimmune interactions, and behavior. From a therapeutic perspective, these tools could serve as a foundation

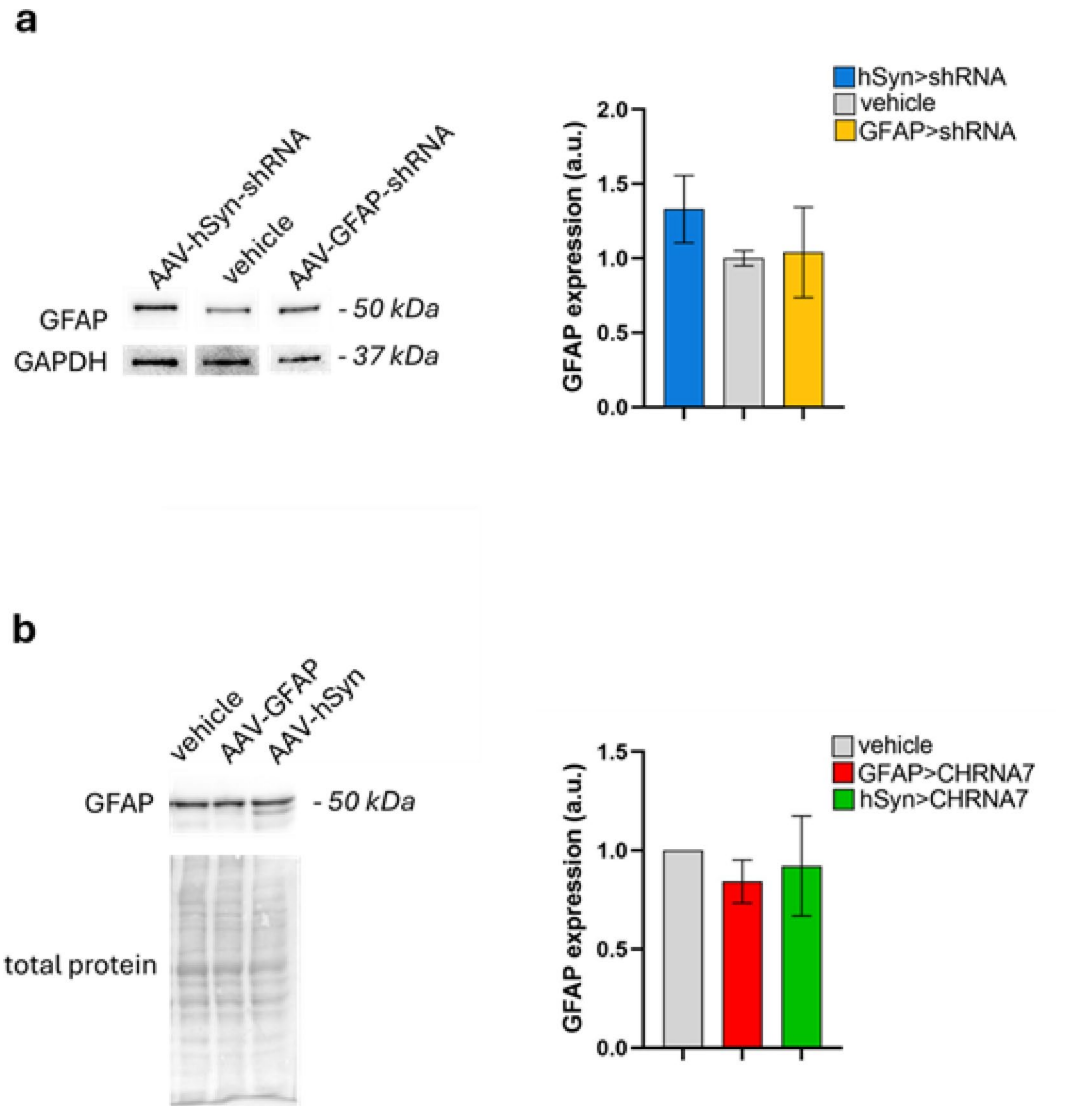

Fig. 5. AAVs infection does not induce significant astrogliosis. Representative WB analysis and relative bar graph showing GFAP levels in primary co-cultures of neurons and astrocytes infected with AAV-PHP.eB-GFAP-shRNA_CHRNA7-GFAP-mRuby2 or AAV-PHP.eB-hSyn-shRNA_CHRNA7-hSyn-mRuby2 (a, the three different lanes derived from the same cropped blot, see Supplementary information - uncropped gels) as well as in hippocampi of mice infected with AAV-PHP.eB-GFAP-CHRNA7-mRuby2 or AAV-PHP.eB-hSyn-CHRNA7-mRuby2 (b, see Supplementary information for uncropped gels). GAPDH and Ponceau S Solution were used as loading controls. The graph shows the results obtained by three independent experiments.

for gene therapy approaches aiming to restore α7-nAChR function in conditions such as Alzheimer's disease[29], schizophrenia[30], or post-stroke cognitive impairment[31].

Future studies will benefit from extending these findings by systematically characterizing the functional consequences of α7-nAChR modulation in vivo, including electrophysiological analyses, behavioral assays, and assessments of neuroinflammatory markers. Moreover, the potential of systemic administration to achieve widespread CNS targeting with similar specificity warrants further investigation. In summary, our work provides a validated toolkit for precise manipulation of α7-nAChR expression in neurons and astrocytes, offering a versatile platform to explore receptor function and develop targeted therapeutic interventions for neurological disorders characterized by receptor dysregulation.

Data availability

The datasets generated and/or analysed during the current study are available in the GenBank-BankIt repository, PV974974.

Received: 17 July 2025; Accepted: 25 March 2026
Published online: 01 April 2026

References

1. Cheng, Q. & Yakel, J. L. The effect of α7 nicotinic receptor activation on glutamatergic transmission in the hippocampus. *Biochem. Pharmacol.* **97**, 439–444 (2015).
2. Ondrejcak, T. et al. Activation of α7 nicotinic acetylcholine receptors persistently enhances hippocampal synaptic transmission and prevents Aß-mediated inhibition of LTP in the rat hippocampus. *Eur. J. Pharmacol.* **677**, 63–70 (2012).
3. Patel, H., McIntire, J., Ryan, S., Dunah, A. & Loring, R. Anti-inflammatory effects of astroglial α7 nicotinic acetylcholine receptors are mediated by inhibition of the NF-κB pathway and activation of the Nrf2 pathway. *J. Neuroinflammation* **14**, 192 (2017).
4. Lendvai, B., Kassai, F., Szájli, Á. & Némethy, Z. α7 Nicotinic acetylcholine receptors and their role in cognition. *Brain Res. Bull.* **93**, 86–96 (2013).
5. Wallace, T. L. & Porter, R. H. P. Targeting the nicotinic alpha7 acetylcholine receptor to enhance cognition in disease. *Biochem. Pharmacol.* **82**, 891–903 (2011).
6. Duffy, A. M. et al. Acetylcholine α7 nicotinic and dopamine D2 receptors are targeted to many of the same postsynaptic dendrites and astrocytes in the rodent prefrontal cortex. *Synapse* **65**, 1350–1367 (2011).
7. Jones, C. α7 Nicotinic Acetylcholine Receptor: A potential target in treating cognitive decline in schizophrenia. *J. Clin. Psychopharmacol.* **38**, 247–249 (2018).
8. Koukouli, F. & Maskos, U. The multiple roles of the α7 nicotinic acetylcholine receptor in modulating glutamatergic systems in the normal and diseased nervous system. *Biochem. Pharmacol.* **97**, 378–387 (2015).
9. Thomsen, M. S., Weyn, A. & Mikkelsen, J. D. Hippocampal α7 nicotinic acetylcholine receptor levels in patients with schizophrenia, bipolar disorder, or major depressive disorder. *Bipolar Disord.* **13**, 701–707 (2011).
10. Cannata, B. et al. Functional deletion of α7 nicotinic acetylcholine receptor impairs Ca2+-dependent glutamatergic synaptic transmission by affecting both presynaptic and postsynaptic protein expression and function. *Front. Physiol.* **16**, 1662171 (2025).
11. Wang, Y. et al. The duplicated α7 subunits assemble and form functional nicotinic receptors with the full-length α7. *J. Biol. Chem.* **289**, 26451–26463 (2014).
12. Giering, J. C., Grimm, D., Storm, T. A. & Kay, M. A. Expression of shRNA from a tissue-specific pol II promoter is an effective and safe RNAi therapeutic. *Mol. Ther.* **16**, 1630–1636 (2008).
13. Fakhr, E., Zare, F. & Teimoori-Toolabi, L. Precise and efficient siRNA design: A key point in competent gene silencing. *Cancer Gene Ther.* **23**, 73–82 (2016).
14. Bofill-De Ros, X. & Gu, S. Guidelines for the optimal design of miRNA-based shRNAs. *Methods* **103**, 157–166 (2016).
15. Graham, F. L., Russell, W. C., Smiley, J. & Nairn, R. Characteristics of a human cell line transformed by DNA from Human Adenovirus Type 5. *J. Gen. Virol.* **36**, 59–72 (1977).
16. Jiang, N., Shi, P., Desland, F., Kitchen-Pareja, M. C. & Sumners, C. Interleukin-10 inhibits angiotensin II-induced decrease in neuronal potassium current. *Am. J. Physiol.-Cell Physiol.* **304**, C801–C807 (2013).
17. Cadwell, C. R. et al. Electrophysiological, transcriptomic and morphologic profiling of single neurons using Patch-seq. *Nat. Biotechnol.* **34**, 199–203 (2016).
18. Wu, H. et al. Improved siRNA/shRNA functionality by mismatched duplex. *PLoS ONE* **6**, e28580 (2011).
19. Sun, G. et al. Differences in silencing of mismatched targets by sliced versus diced siRNAs. *Nucleic Acids Res.* **46**, 6806–6822 (2018).
20. Renna, P. et al. Engineering a switchable single-chain TEV protease to control protein maturation in living neurons. *Bioeng. Transl. Med.* **7**, (2022).
21. Ripoli, C. et al. Engineering memory with an extrinsically disordered kinase. *Sci. Adv.* **9**, eadh1110 (2023).
22. Li Puma, D. D. et al. Extracellular tau oligomers affect extracellular glutamate handling by astrocytes through downregulation of GLT-1 expression and impairment of NKA1A2 function. *Neuropathol. Appl. Neurobiol.* **48**, e12811 (2022).
23. Guo, Y. et al. High-titer AAV disrupts cerebrovascular integrity and induces lymphocyte infiltration in adult mouse brain. *Mol. Ther. Methods Clin. Dev.* **31**, 101102 (2023).
24. Liu, S. et al. Structural basis for allosteric agonism of human α7 nicotinic acetylcholine receptors. *Cell Discov.* **11**, 35 (2025).
25. Letsinger, A. C., Gu, Z. & Yakel, J. L. α7 nicotinic acetylcholine receptors in the hippocampal circuit: Taming complexity. *Trends Neurosci.* **45**, 145–157 (2022).
26. Xu, Z.-Q., Zhang, W.-J., Su, D.-F., Zhang, G.-Q. & Miao, C.-Y. Cellular responses and functions of α7 nicotinic acetylcholine receptor activation in the brain: A narrative review. *Ann. Transl. Med.* **9**, 509–509 (2021).
27. Mathiesen, S. N., Lock, J. L., Schoderboeck, L., Abraham, W. C. & Hughes, S. M. CNS transduction benefits of AAV-PHP.eB over AAV9 are dependent on administration route and mouse strain. *Mol. Ther.* **19**, 447–458 (2020).
28. Chan, K. Y. et al. Engineered AAVs for efficient noninvasive gene delivery to the central and peripheral nervous systems. *Nat. Neurosci.* **20**, 1172–1179 (2017).
29. D'Andrea, M. & Nagele, R. Targeting the alpha 7 nicotinic acetylcholine receptor to reduce amyloid accumulation in Alzheimers disease pyramidal neurons. *Curr. Pharm. Des.* **12**, 677–684 (2006).
30. Martin, L. F., Kem, W. R. & Freedman, R. Alpha-7 nicotinic receptor agonists: potential new candidates for the treatment of schizophrenia. *Psychopharmacology (Berl).* **174**, (2004).
31. Aguado, L. et al. Therapeutic effect of α 7 nicotinic receptor activation after ischemic stroke in rats. *J. Cereb. Blood Flow Metab.* **43**, 1301–1316 (2023).

Acknowledgements

We would like to acknowledge the contribution of the Core Facility G-STeP "Electrophysiology", and Ministero della Salute - Ricerca Corrente 2026 - Fondazione Policlinico Universitario "A. Gemelli" IRCCS.

Author contributions

Conceptualization: CR, RP, CG; writing original draft preparation: CR; writing review and editing: GP, MB, PR, CR, RP, CG. Methodology: CR, PR, CG. Investigation: GP, MB, PR, RP. Figure preparation: GP, MB, PR, RP. All authors have read and agreed to the published version of the manuscript.

Declarations

Competing interests

The authors declare no competing interests.

Additional information

Supplementary Information The online version contains supplementary material available at https://doi.org/10.1038/s41598-026-46279-2.

Correspondence and requests for materials should be addressed to C.R.